Environmental Science Nano

# Efficient Ammonia Recovery from Wastewater using Electrically Conducting Gas Stripping Membranes



| | |
|---|---|
| Journal: | *Environmental Science: Nano* |
| Manuscript ID | EN-ART-11-2019-001303.R1 |
| Article Type: | Paper |
| | |

This manuscript describes the fabrication, characterization, and testing of an electrically-conducting gas stripping membrane composed of a carbon nanotube/nickel composite. The membrane is used to efficiently extract ammonia from wastewater, which is demonstrated to be more energy efficient than existing treatment methods. Furthermore, this method has the potential of addressing one of the major shortfalls of anaerobic wastewater treatment – its inability to effectively remove nitrogen contamination.

ARTICLE

# Efficient Ammonia Recovery from Wastewater using Electrically Conducting Gas Stripping Membranes

Received 00th January 20xx,
Accepted 00th January 20xx

DOI: 10.1039/x0xx00000x

Arpita Iddya[a], Dianxun Hou [b], Chia Miang Khor[a], Zhiyong Ren[c], Jefferson Tester[d], Roy Posmanik[e], Amit Gross[f] and David Jassby *[a]

Recovery of nutrients, such as ammonia, from wastewater offers an attractive approach to increase the overall sustainability of waste management practices. Conventional wastewater treatment processes require significant energy input, and the useful form of nitrogen (ammonia), is usually lost. Ammonia, a major component of fertilizers, is convetionanlly manufactured using the Haber-Bosch process, which accounts for approximately 2% of worldwide energy demand. A better approach would efficiently capture ammonia directly from the wastewater. In this study, ammonia is recovered directly by using an electrically conducting gas-stripping membrane that is immersed into a wastewater reactor. Under cathodic potentials, these membranes were used to facilitate conversion of ammonium ($NH_4^+$) into ammonia ($NH_3$), which was then extracted by either circulating an acid solution or by applying a vacuum on the back side of the membrane . The mechanism involves water electrolysis, which generates $OH^-$, and transforms ammonium to ammonia that is stripped through the membrane. By engineering the surface and transport properties of the membrane 68.8±8.0 g-N/m$^2$/d of ammonia was recovered, with an energy consumption of 7.1±1.1 kWh/kg-N.

## Introduction

Increasing interest in process sustainability and a growing water and resource scarcity are driving the need for recovery of valuable resources from wastewater streams.[1–4] Wastewater is a potentially attractive source of clean water and nutrients.[5] High-strength wastewater streams contain large amounts of organic matter and nutrients, such as nitrogen (N) and phosphorus (P), that are essential for the growth and development of organisms, and can, if released in excess, lead to eutrophication in receiving water bodies.[6] Therefore, the removal and recovery of nutrients from wastewater streams serves a dual purpose, eliminating a eutrophication source while simultaneously providing a source of fertilizer and/or energy.[7,8] In addition, nutrient recovery is attractive (compared to simple transformation of said nutrients to $N_2$ gas, e.g., through nitrification/denitrification) because it (i) mitigates the environmental footprint of wastewater treatment processes, and (ii) leads to decreased fossil fuel use for the production of synthetic fertilizers.[9] Thus, harvesting and using nutrients from wastewater can lead to potentially significant environmental, economic, and energy savings, increasing the overall sustainability of the wastewater treatment process. [10–13] The economic prospects of this process could be enhanced by implementing clean energy incentives, such as carbon credits.

Conventional water treatment relies on biological processes (nitrification, denitrification, or anammox) to remove N contamination.[6,14]. There are two main drawbacks to this process. First, in raw wastewater, N is primarily found in its useful form, ammonium ($NH_4^+$). During the nitrification and denitrification process, ammonium is converted to $N_2$, which is lost to the environment. Nitrogen is then used in the energy-intensive Haber-Bosch process to generate ammonia (which is

[a.] Department of Civil and Environmental Engineering, University of California, Los Angeles, California 90095, United States
[b.] Department of Civil, Environmental and Architectural Engineering, University of Colorado Boulder, Boulder, Colorado 80303, United States
[c.] Department of Civil and Environmental Engineering, Princeton University, Princeton, New Jersey 08544, United States
[d.] Department of Chemical and Biomolecular Engineering and Energy Systems Institute, Cornell University, Ithaca, New York 14853, United States
[e.] Agricultural Research Organization - Volcani Center, Newe Ya'ar Research Center, Ramat Yishai, 30095, Israel
[f.] Zuckerburg Institute for Water Research, Ben-Gurion University of Negev, Sede Boqer Campus, 84990, Israel

converted to ammonium when dissolved in water). Largely as a result of reforming natural gas to produce the required hydrogen for ammonia synthesis, the Haber-Bosch process accounts for approximately 2% of global primary energy consumption. [15,16] Second, the nitrification/denitrification process, which is a biological process with an initial aerobic phase (nitrification), requires significant energy investment, primarily in the form of aeration.[17] Moreover, $N_2O$, a potent greenhouse gas, is released during both processes.[4,18] Therefore, the current method of treating N contamination in waste streams requires energy to first convert ammonium to an inert form ($N_2$), which then requires further energy input to re-convert it back to ammonia. A better approach would allow the capture of this ammonium directly from the waste stream (ideally in pure form), which would eliminate the need for nitrification, as well as decrease the need to convert atmospheric $N_2$ to ammonia. Another important advantage to the direct capture of ammonium from wastewater involves the removal of organic contaminants. Currently, the dominant process for organic removal is the activated sludge process, which is energy intensive (due to its aerobic nature) and generates large amounts of biosolids.[19,20] Anaerobic treatment of wastewater is an attractive option due to its small energy footprint, its ability to generate energy (in the form of methane), and the small amount of biosolids generated.[21,22] However, the adoption of anaerobic treatment of ammonium-rich streams is hindered by anaerobic bacteria's low N-removal capacity.[23–25] Therefore, developing a N-removal method that is compatible with anaerobic processes could potentially transform wastewater treatment across multiple sectors.[24]

Many studies have investigated ammonium removal and recovery from waste streams by non-biological methods, including reverse osmosis, air/vacuum stripping, zeolite adsorption, ion exchange, struvite precipitation, and electrodialysis.[26–32] However, these processes have drawbacks, such as high energy demand and chemical input requirements. For example, air and vacuum stripping, and struvite precipitation, require lime addition to increase alkalinity and/or elevated temperatures[33–35]; reverse osmosis membranes struggle with low selectivity, and ion exchange materials are expensive and experience a drop in performance from the presence of competing ions.[36–38]

In an aqueous solution, ammonia and ammonium are in a pH dependent equilibrium, according to the following equation[35]:

$$NH_4^+ + OH^- \leftrightarrow NH_3 + H_2O, \quad pK_a = 9.246 \qquad (1)$$

Where ammonia dominates in aqueous alkaline media with pH>10.[39] While the solubility of ammonium is extraordinarily high in water (the solubility of $NH_4Cl$ in water at 25 °C is 383 g/L), the solubility of ammonia is lower ($k_H$ = 0.59 mol $m^{-3}$ $Pas^{-1}$).[14,40,41] Therefore, shifting the solution pH towards more basic conditions will convert ammonium to ammonia, and enable the extraction of ammonia vapor.[14,15,26,40–44] Chemically-assisted $NH_3$ extraction through the addition of CaO, $Ca(OH)_2$, and NaOH, which raises the pH of the solution and shifts $NH_4^+$ to $NH_3$, has been demonstrated by several earlier studies.[26,35,41,45,46] An electrochemically-driven pH shift has also been previously demonstrated.[47] Christaens et al. (2017) used a (bio)electrochemical system to produce hydroxide ions at the cathode, and convert $NH_4^+$ ions to $NH_3$ which were then removed via gas stripping.[47] Similarly, Zhang et al. (2017) used flow-electrode capacitive deionization process to facilitate

 

accumulation of ammonium ions in the cathode where an increase in pH due to water splitting would favor the presence of ammonia over ammonium ions.[48] The extraction of ammonia from an aqueous stream has been achieved by inducing a partial vapor pressure difference between two streams. For example, Hou et. al. and Tarpeh et. al. used a hydrophobic membrane separating an ammonia-rich feed solution from a highly acidic draw solution, which provided an ammonia sink.[18,49] Increasing the temperature of the ammonia-rich solution also enabled the extraction of ammonia through either a hydrophobic membrane or the reactor's head- space.[35,43,50] In particular, vacuum-based extraction of ammonia is an attractive method, as the resulting ammonia is in relatively pure form, which can be used for more desired applications (e.g., energy generation) than fertilizer.[26] However, the high solubility of ammonia necessitates high vacuum pressures to induce effective extraction.[26,35]

In this study, we fabricated a novel electrically conducting gas stripping electrode by coating a hydrophobic polymeric support membrane with a layer of nickel-functionalized carbon nanotubes (CNTs). The gas-stripping electrodes are used as cathodes in a half-cell that is separated from a simulated high-strength wastewater (the anolyte) by a cation exchange membrane (CEM). As demonstrated by previous work in this area using this setup, ammonium from the wastewater migrates in response to an electric field across the CEM. Water electrolysis in the catholyte increases the local pH, which shifts the ammonium to ammonia that is subsequently extracted through the membrane.[15,18,47,49]

We provide extensive membrane characterization and demonstrate very high ammonia recovery. Driving force for the extraction is provided through either circulating an acidic solution on the backside of the membrane, or through a vacuum. We also discussed the impact of electrode surface and physical properties on system performance, as well as described the impact of the driving force on the energy intensity and efficiency of the process.

## Materials and Methods

**Materials and Chemicals** A commercial hydrophobic polytetrafluoroethylene (PTFE) membrane (0.22 μm, Sterlitech, Kent, WA) was used for this study. Multiwall CNTs (outer diameter: 13-18nm, length: 3-30 μm, purity >99%, and functional group content[15] of 7%) functionalized with carboxylic groups via plasma treatment were purchased from CheapTubes Inc. (Brattleboro, VT). Sodium dodecylbenzenesulfonate (DDBS, technical grade, Sigma Aldrich), nickel sulfate heptahydrate ($NiSO_4.7H_2O$, 98% Alfa Aesar), nickel chloride hexhydrate ($NiCl_2.6H_2O$, reagent grade, Sigma Aldrich), boric acid ($H_3BO_3$, ACS grade, Fisher), sulfuric acid ($H_2SO_4$, 96.5%, Fisher), dextrose (ACS grade, Fisher), ammonium sulfate ($(NH_4)_2SO_4$, ACS grade, Fisher), ammonium bicarbonate ($NH_4HCO_3$, 99%, Acros Organics), potassium phosphate monobasic ($KH_2PO_4$, ACS grade, Fisher), potassium sulfate ($K_2SO_4$, ACS grade, Fisher), magnesium sulfate heptahydrate ($MgSO_4.7H_2O$, ACS grade, Fisher), calcium sulfate dihydrate ($CaSO_4.2H_2O$, 98%, Acros Organics), and sodium chloride (NaCl, ACS grade, Fisher) were used as received.

**Solution Preparation** The CNT spray coating solution was composed of 0.1 wt% CNT powder dispersed in DI water, stabilized using DDBS at a 1:10 (CNT: DDBS) ratio. The electrodeposition solution for Nickel deposition contained 150 mM $NiSO_4.7H_2O$, 25 mM $NiCl_2.6H_2O$, and 500 mM $H_3BO_3$ (at pH 2.00, adjusted using $H_2SO_4$).[18]

The synthetic wastewater (anolyte) was composed of 55.5 mM dextrose; 5.2 mM $(NH_4)_2SO_4$; 43 mM $NH_4HCO_3$; 4.7 mM $KH_2PO_4$; 8.51 mM $K_2SO_4$; 5.89 mM $MgSO_4.7H_2O$; 3.23 mM $CaSO_4.2H_2O$; 0.21 mM $Na_2SO_4$ in millipure water.[51] Chloride-containing salts were avoided in the anolyte to eliminate the possible formation of chlorine (through chloride oxidation on the anode) that can form chloramines and complicate the analysis of the fate of ammonium in the system; although not representative of many actual wastewater steams, the absence of chloride salts eliminated concerns about alternate pathways for ammonium transformation.[52] In wastewaters containing chlorides, chloramine formation may occur, which can reduce the amount of ammonia that can be recovered. The total electrical conductivity and pH of the feed were 7.51 dS/m, and 7.48 respectively. The catholyte was composed of 0.0705M NaCl and 0.0278M $(NH_4)_2SO_4$ (pH of 7.04) in deionized water.

**Membrane Preparation and Characterization** The CNT-coated electrically conducting membrane (ECM) was prepared as previously described by Li et al.[53] In short, CNT powder was suspended in solution using a horn sonicator, followed by centrifugation at 11,000 rcf (Avanti J-E Centrifuge, Beckman Coulter; Brea, CA) in two 10 min cycles to remove unsuspended particulates. The CNT suspension was spray-coated onto the PTFE membrane support to achieve a thickness of approximately 1 µm. The prepared membrane was washed overnight with deionized (DI) water to remove residual DDBS, and then dried in the oven at 90 ºC for 15 min.

To deposit Nickel onto the membrane, the membrane was taped onto a stainless steel (SS) mesh with a mesh opening size of 0.222" to provide better electrical contact and to minimize the voltage drop across the CNT surface. The membrane-mesh composite was immersed in the electroplating bath and connected to an external power source (Korad KA3005P DC power supply), with the membrane used as cathode and a Ni 200 plate used as anode. The deposition was carried out under constant current conditions (20.4 $A/m^2$) for 6h (6h-Ni) or 24h (24h-Ni). The prepared Ni coated ECMs were peeled off the SS mesh, rinsed with DI water to remove any Ni residue and dried in an oven at 90 ºC. The 6 and 24h ECMs had a nickel loading of 2.83±0.08 mg/$cm^2$ and 15.71±2.61 mg/$cm^2$, respectively.

The hydrophilicity of the ECM surfaces was determined by contact angle measurements (CA; model 250, Rame-hart; Succasunna, NJ). Surface morphology was imaged using scanning electron microscopy (SEM; ZEISS Supra 40VP SEM; Oberkochen, DE) and evaluated for surface roughness (as the root mean square roughness) using ScanAsyst-Air and probes (Camarillo, CA) by Atomic Force Microscopy (AFM; Bruker Dimension FastScan Scanning Probe Microscope; Billerica, MA). X-ray photoelectron spectroscopy (XPS; Kratos Axis Ultra DLD spectrometer equipped with a monochromatic Al Kα X-ray source) was used to characterize the elemental composition of the membrane surface. The permeance of the membrane was measured using a bubble flow meter. The sheet resistance and conductivity of the membrane were determined using a four-point probe (Veeco; Plainview, NY) and cyclic voltammetry (CV). CV was done using a three electrode electrochemical analyzer (Potentiostat; CH Instruments 6005E; Austin, TX). A potential range of -1.2 to 0 V vs Ag/AgCl was applied to the ECMs as the working electrode at a scan rate of 0.01 V/s. A platinum wire was used as the counter electrode and all three electrodes were immersed in synthetic feed solution.

**Experimental Setup** Experiments were conducted using a two-chamber cell with the chambers separated by a CEM (active membrane area 5.5 cm X 8 m, Fumasep FKE-50, Fuel Cell Store). A platinum coated titanium mesh placed 8 cm away from the CEM was used as an anode, while the ECM placed 5 cm away from the CEM and used as the cathode (Figure S1a-b).

Two experimental setups were used to provide the driving force for ammonia extraction. In the first setup, a 0.01M $H_2SO_4$ solution was circulated along the back-side of the membrane with a flow rate of 0.026 LPM (Figure S1a); this solution acts as an ammonia sink, providing a partial vapor pressure gradient that draws ammonia from the catholyte to the acid solution.[41,54] In the second setup, a vacuum pressure of -29 inHg (VE 225, 2 stage vacuum pump, 3.0 CFM) was continuously applied to the back of the membrane, which stripped dissolved ammonia through the membrane (Figure S1b). The vacuum stream carrying ammonia from the permeate chamber was directed into an acid trap containing 0.01M $H_2SO_4$ to convert ammonia into ammonium and prevent escape into the vacuum pump. The acid trap was followed by a water trap to capture any residual ammonia or acid vapors, followed by a desiccator to prevent water vapor from entering the vacuum pump. Each experiment was conducted as a batch experiment for a duration of 6h for each ECM as well as each experimental setup.

The ECM was housed in a custom-built flow cell (Figure S1c) with the membrane sandwiched between a frame and a bottom chamber. The ECM was placed such that the active surface (with CNT and/or Ni) faces the solution and the permeate side faces the cell bottom. The frame exposes an active area of the ECM (36 mm X 60 mm) directly to the solution, while the bottom part of the flow cell acts as a permeate chamber to pass acid solution or apply vacuum. An aluminium shim, cut to expose the active area of the membrane, was placed over the ECM to provide better electrical contact and to connect the ECM to the potentiostat. The entire flow cell was immersed into the cathode chamber (volume = 0.5L) along with the reference electrode while the anode was placed in the anode chamber (volume = 1.5L).

**Operating Conditions** Both anode and cathode compartments were continuously stirred using magnetic stirrers. In our experiments, three types of membranes were evaluated: CNT-only, 6h-Ni, and 24h-Ni. To induce electromigration of ammonium from the anolyte to the catholyte and promote water electrolysis on the ECM, a constant DC cathodic potential of 1.2 V vs. Ag/AgCl was applied to the membrane surface using a three-electrode potentiostat (CH Instruments 6005E, Austin, TX). The pH of the anolyte and catholyte was measured throughout the experiment using a pH probe. 10 mL samples were periodically collected from each of the three solutions (anolyte, catholyte, and acid stripping solution) and analyzed for $NH_4^+$ ion concentration using an ammonia ion selective electrode (Orion™ High performance ammonia electrode, ThermoFisher; Waltham, MA). The presence of possible ammonium transformation products (e.g., nitrate, nitrite, chloramines) were evaluated by testing the samples for total nitrogen and nitrate concentrations using total nitrogen analysis (TOC/TN analyzer, Shimadzu; Kyoto, JP) and a spectrophotometer (HACH DR1900, Loveland, CO), respectively.

The ammonia transport rate, ammonia removal rate, recovery rate, specific energy consumption and recovery were used to evaluate the process:

$$Ammonia\ transport\ rate = \frac{N_{A0} - N_{Aend}}{A_{CEM} * t} \quad (2)$$

$$Ammonia\ removal\ rate = \frac{N_{T0} - N_{Tend}}{A_m * t} \quad (3)$$

$$Ammonia\ recovery\ rate = \frac{M_{end} - M_0}{A_m * t} \quad (4)$$

$$Specific\ energy\ consumption = \frac{(V * I * t)}{M_{end} - M_0} \quad (5)$$

$$Recovery\ = \frac{M_{end} - M_o}{N_{T0} - N_{Tend}} * 100 \quad (6)$$

where, $N_{A0}$ and $N_{Aend}$ are the initial and final mass of ammonia-nitrogen in the anode respectively, $N_{T0}$ and $N_{Tend}$ are the total initial and final mass (in the anolyte and catholyte combined) of ammonia-nitrogen ($NH_3$-N) respectively, $M_0$ and $M_{end}$ are the initial and final mass of $NH_3$-N in the acid solution, $A_m$ is the area of the ECM, $A_{CEM}$ is the area of the CEM, t is the duration of the experiment, V is the potential applied, and I is the current during the experiment. Here, removal rate is defined as the total amount of ammonia removed from the system (anolyte and catholyte), which includes the ammonia recovered across the ECM and the ammonia lost from the system (e.g., due to volatilization to the headspace), and recovery rate is the rate of ammonia transfer across the CEM.

## Results and discussion

### Membrane Characterization

The addition of a CNT coating to the surface of a hydrophobic PTFE membrane creates a black surface (Figure 1a); once the CNT network undergoes the Ni deposition step, the surface takes on a silvery sheen, indicative of the presence of a metal coating, with the longer Ni deposition time (24h) leading to a more complete-looking metal coverage (Figure 1b-c). Importantly, membranes undergoing nickel deposition for less than 6 hours showed incomplete metal coverage (not shown). Figures 1(d-f) shows the contact angle images of the three membranes. The CNT membrane is most hydrophobic with a contact angle of 146±8º (Figure 1d). Nickel deposition increases hydrophilicity of the membrane surface as seen by the contact angles for 6h-Ni (93±3º) and 24h-Ni (83±6º). Figures 1(g-i) show the membrane's surface as imaged by SEM. Prior to Ni deposition, CNTs are readily visible to form a uniform dense and porous network on the membrane surface with a pore size of about 0.1-0.2 µm (Figure 1g). Following a 6-h Ni deposition step, a rough-looking metallic cover can be seen to have grown on the CNT surface (Fig. 2h); the longer Ni deposition time (24 h), led to a rougher looking surface cover (Fig. 2i). Cross-sectional SEM micrographs of the membranes, show the thickness of the layers to be 1.57±0.49 µm (CNT), 2.99±0.60 µm nickel after 6h of electrodeposition (6h-Ni), and 22.49±3.45 µm nickel after 24h of electrodeposition (24h-Ni) (Figure 1j-l). Thus, structure and depth of the Ni layer can be manipulated by varying the Ni deposition time. The root mean square roughness,

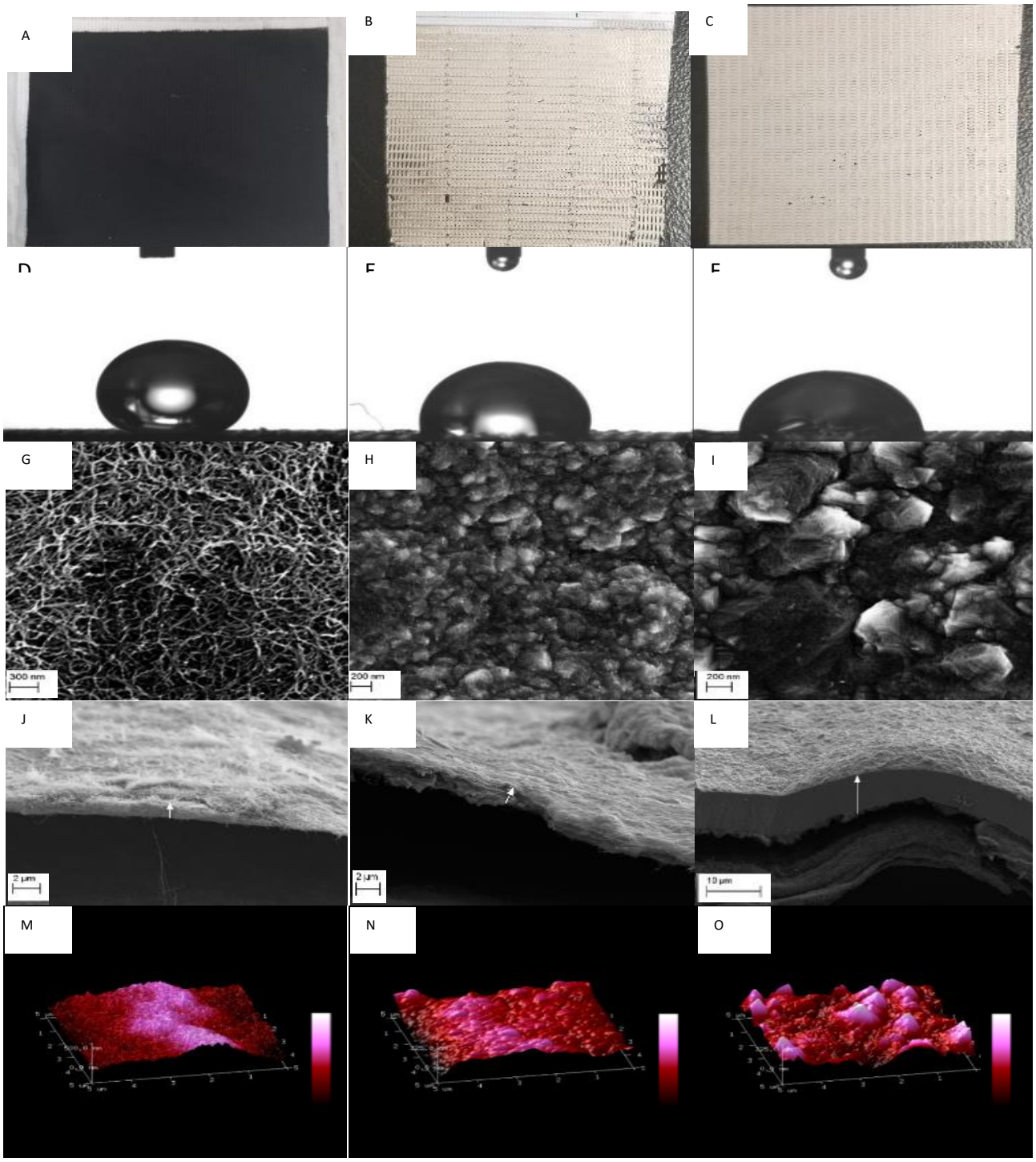


**Figure 1:** Photographs of A) CNT-coated ECM, B) ECM with Nickel deposited on CNT for 6h (6h-Ni), and C) ECM with Nickel deposited on CNT for 24h (24h-Ni); contact angle measurements of D) CNT- coated PTFE membrane, E) ECM with Nickel deposited on CNT for 6h (6h-Ni), and F) ECM with Nickel deposited on CNT for 24h (24h-Ni); SEM micrographs of G) CNT-coated PTFE membrane, H) ECM with Nickel deposited on CNT for 6h (6h-Ni), and I) ECM with Nickel deposited on CNT for 24h (24h-Ni); cross-sectional SEM micrographs of J) CNT-coated PTFE membrane, K) ECM with Nickel deposited on CNT for 6h (6h-Ni), and L) ECM with Nickel deposited on CNT for 24h (24h-Ni); AFM images of a 5µm x 5µm section of M) CNT-coated PTFE membrane, N) ECM with Nickel deposited on CNT for 6h (6h-Ni), and O) ECM with Nickel deposited on CNT for 24h (24h-Ni).

characterized by AFM, of a 5µm x 5µm segment of CNT coated membrane was 133±2 nm (Figure 1m). The 6h Ni deposition process reduced surface roughness to 63.3±2.90 nm (Figure 1n), while the 24h Ni deposition yielded a surface roughness of 82.7±3.78 nm (Figure 1o).

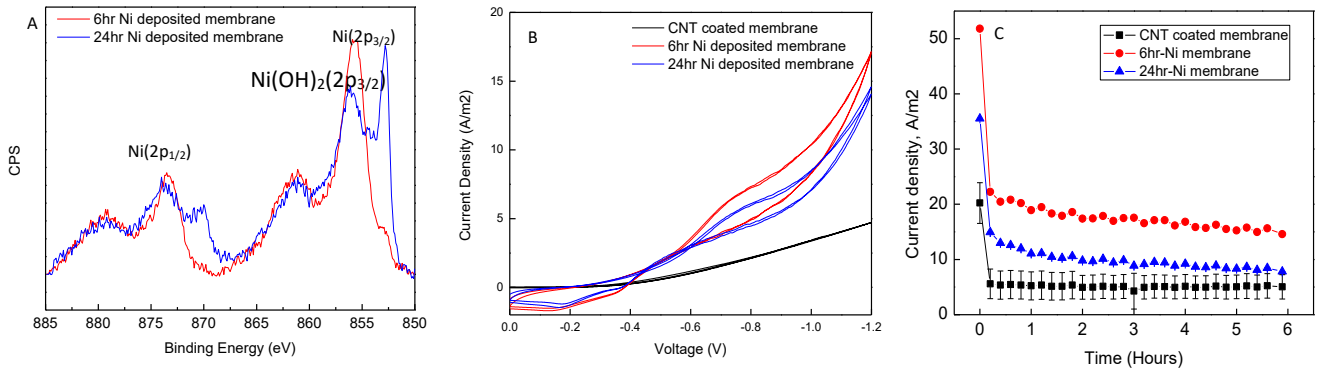


**Figure 2**: A) XPS spectra of 6h-Ni and 24h-Ni membranes showing Ni(0) and Ni(OH)2 2p peaks. B) CV curves of the three ECMs, obtained at a scan rate of 0.01 V/s. C) Time course change in current during the experiments.

The sheet resistance of the CNT coated membrane was determined to be 47.59 Ω/□, while for the nickel membranes the resistance declined to 5.91 Ω/□ (6h-Ni) and 0.01 Ω/□ (24h-Ni). Thus, introducing Ni on membrane surface dramatically decreased sheet resistance. Gas permeability measurements of the two nickel membranes revealed their permeance to be 48,000±7,743 barrer for the 6h-Ni and 18,000±5,443 barrer for 24h-Ni, which is 60-90% lower than traditional polymeric membranes[55,56], indicating that the addition of the Ni coating does indeed constrict the flow of gasses through the membrane, possibly due to pore constriction.

XPS was conducted to study the elemental composition of the membrane surface once Ni was deposited. Figure 2a shows the XPS spectra of the Ni($2p_{1/2}$) and Ni($2p_{3/2}$) bands and their satellites for the 6h-Ni and 24h-Ni membranes. The 24h-Ni membrane shows peaks at 852.7 eV and 856 eV, which correspond to Ni(0) and Ni(2+) as $Ni(OH)_2$, respectively. The 6h-Ni membrane shows a pronounced peak for Ni(2+) as $Ni(OH)_2$, and a weak peak for Ni(0).[57–60] It is possible that the smaller Ni(0) peak observed in the 6h-Ni sample is a result of extensive oxidation of the deposited Ni, a result of atmospheric exposure. In contrast, the thicker Ni cover obtained after 24h deposition may provide better oxidation protection, resulting in more abundant Ni(0).[18,61]

The electrochemical properties of the membranes were characterized using current density versus voltage (CV) measurements (Figure 2b). Nickel is known to reduce the over-potential associated with the hydrogen evolution reaction (HER). [62–66]. To compare the activities of the different ECM materials, we measured the onset potential, defined as the potential at which the electron transfer process for a specific redox reaction begins, translated as an increase in current (Figure 2b).[67] For the HER, the onset of hydrogen evolution gives us insight into the catalytic activity of the surface under study.[68] The CNT ECM shows an onset potential of -0.4 V vs. Ag/AgCl. The 6h Ni and the 24h Ni ECMs have lower onset potentials of -0.24 and -0.2 V vs. Ag/AgCl, respectively. The current at -1.2V for the CNT ECM was 4.7 A/$m^2$, while for 6h and 24h Ni ECMs the current at -1.2 V was 17 and 14.5 A/$m^2$ respectively. The higher current at 1.2V for the 6h Ni ECM could be associated to its surface structure. The 6h Ni ECM surface has many small peaks and is more porous as compared to the 24h Ni ECM (which has fewer, more pronounced peaks). Many studies have shown that the edges of $Ni(OH)_2$ promotes water dissociation. Thus, the surface morphology of the 6h Ni ECM could be

responsible for the higher observed current and more efficient HER.[57]

**Ammonia Recovery Using Acid Stripping Solution**

When the 0.01 M $H_2SO_4$ solution was used as the driving force for ammonia transport across the ECM, the ammonia removal and recovery rate were highest for the 6h Ni ECM, with a removal of 109± 21.55 g-N/m$^2$/d and recovery of 68.8± 8.02 g-N/m$^2$/d. The 24h Ni ECMs exhibited a removal of 99.5± 55.15 g-N/m$^2$/d and recovery of 20.5± 3.68 g-N/m$^2$/d. The CNT coated ECMs showed ammonia removal of 30.3± 6.32 g-N/m$^2$/d and ammonia recovery of 20.7± 8.15 g-N/m$^2$/d. In all cases, a cathodic potential of 1.2 V vs. Ag/AgCl was applied to the ECM. The current in the experiment decreased with time for each ECM (Figure 2c). The current decline could be attributed to the increase in cathodic overpotential as the pH in the catholyte increases with time due to accumulation of $OH^-$.[18]

Ammonia removal and recovery can be explained by looking at the mechanism for ammonia transport and removal. Ammonia recovery in the system occurs in three steps[26]:

i. $NH_4^+$ transport from anode to cathode across the CEM.
ii. Transformation of $NH_4^+$ to dissolved $NH_3$ in catholyte (eq. 1).
iii. $NH_3$ transport from the catholyte into the permeate chamber across the ECM.

**Transport across CEM** The application of a potential produces a current that leads to electromigration of ions toward the oppositely charged electrode.[69] Effective recovery of $NH_3$-N depends on the efficiency of its transport across the CEM from the anolyte to catholyte. The efficiency of $NH_3$-N transport across the CEM depends upon current density, total ammonia nitrogen (TAN) loading rate, pH and continuous removal of ammonia from the catholyte chamber. Since migration of the ions is current driven, it is important to consider the ratio between current density and TAN loading, termed the load ratio. Load ratio is the ratio of the applied current density to the theoretical amount of charge transported across the CEM as $NH_4^+$ (eq. 7):[70]

$$L_N = \frac{j_{applied}}{C_{A0} * Q_A * \frac{F}{A_{CEM}}} \quad (7)$$

Where, $j_{applied}$ is the applied current density (A/m$^2$), $C_{A0}$ is the initial molar concentration of the anode (mol/m$^3$), F is the Faraday constant (96.485 C/mol), $A_{CEM}$ is the surface area of the CEM (0.004 m$^2$), and $Q_A$ is the anolyte inflow rate (m$^3$/s). For our batch system, $Q_A$ is calculated as the volume of anolyte (m$^3$) divided by the duration of the experiment (s). The significance of the load ratio is understood by looking at its absolute value: $L_N$ <1, implies more N is fed to the system (i.e., a low current that cannot remove ammonia), whereas $L_N$>1, implies that the produced current is sufficiently high to induce $NH_4^+$ transport.

In our system, $L_N$ was calculated to be in the range of 0.1 (CNT)-0.3 (6h-Ni & 24h-Ni), implying that ammonia transport across the CEM is limited by electrical current.[70,71] This low $L_N$ value suggests that higher current densities may increase the transport of ammonium across the CEM, which would increase ammonium removal.

Mass transport across the CEM results in a decrease in mass of $NH_3$-N in the anode chamber and an increase in the cathode chamber (Figure 3a, b). In the anode chamber, the mass of $NH_3$-N decreases from 942.58 ± 29.27 mg to 811.08 ± 39.44 mg when the CNT ECM was used as the cathode. For Nickel ECMs, the mass of $NH_3$-N decreased from 1034.52 ± 24.95 mg to 856.55 ±

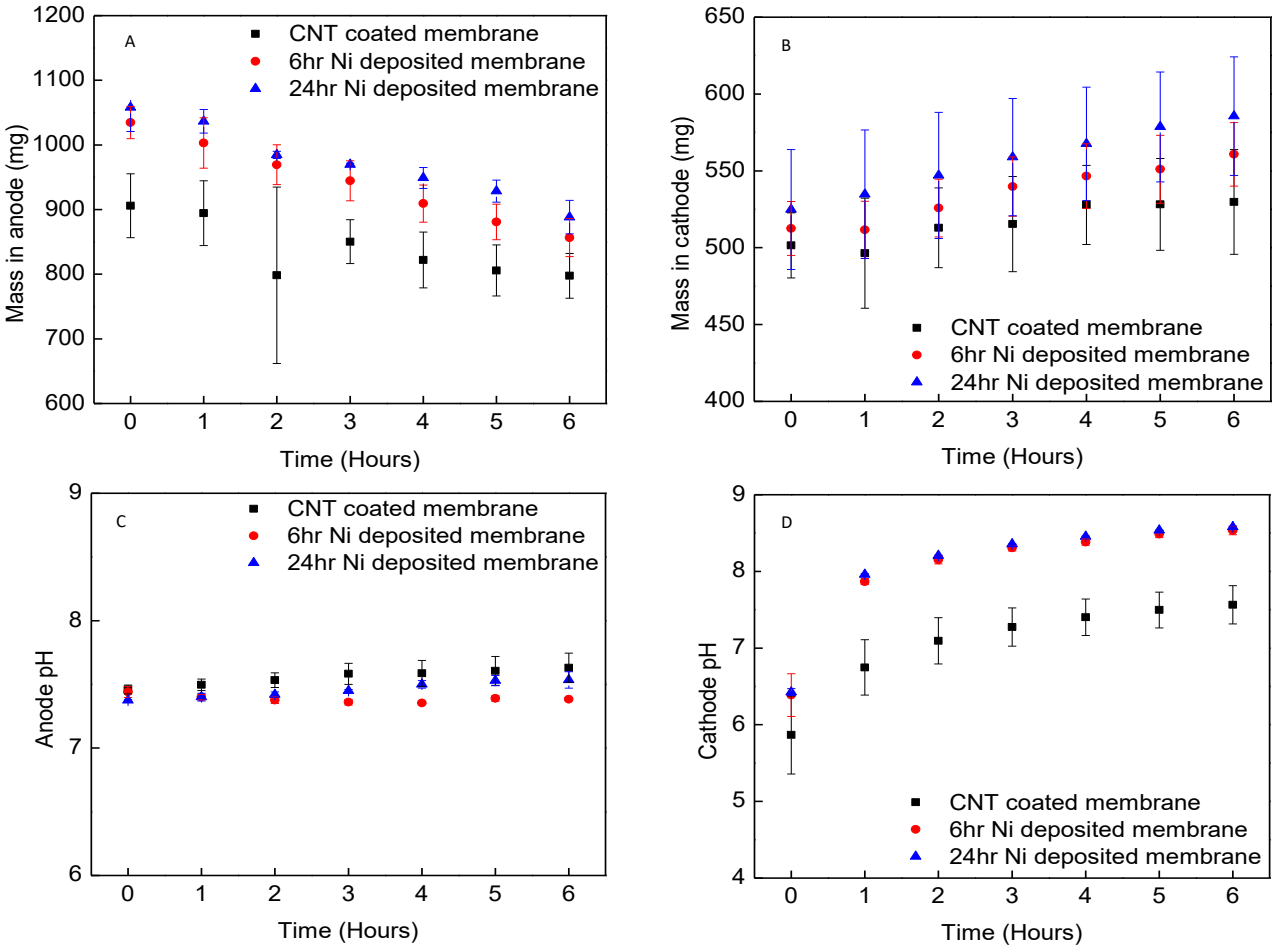


**Figure 3**. Change of mass of $NH_3$-N over time in the a) anolyte and b) catholyte chambers. pH change over time in the c) anolyte and d) catholyte chambers. The error bars in figure represent the standard deviation.

29.47 mg for 6h-Ni, and from 1050.67 ± 32.12 mg to 868.01 ± 35.65 mg for the 24h-Ni materials. Ammonia flux across the ECM can be seen in Fig. S2. Due to low the low current in the CNT ECM setup, the $NH_3$-N transport rate across the CEM was also the lowest (111.76 ±36.87 g-N/m$^2$/day), while for the nickel membranes the transport was similar (177.96 ±13.77 g-N/m$^2$/day for 6h-Ni and 182.66 ±20.50 g-N/m$^2$/day for 24h-Ni membrane). The decrease in $NH_3$-N concentrations in the anode chamber is accompanied by a corresponding increase in the $NH_3$-N concentrations in the cathode chamber. For CNT ECMs, the mass of $NH_3$-N increased from 500.70 ±22.14 to 529.77 ± 34.10 mg, while for 6h-Ni membrane, the mass of $NH_3$-N increased from 512.54 ± 17.55 to 560.75 ± 20.73 mg, and from 512.14 ± 36.60 to 567.63 ± 40.47 mg for 24h-Ni ECMs. We verified the data generated using the ammonia selective electrodes using a colorimetric method (using a HACH kit) (data not shown).

While the $NH_3$-N removal from the cathode chamber was approximately 20%, it is important to note that the overall removal of membrane-based processes is surface area dependent. Therefore, to achieve higher removal of $NH_3$-N in real systems (where certain removal thresholds must be met), larger membrane areas would be needed.

The migration of $NH_4^+$ from the anolyte to the catholyte was driven by the electric field generated between the anode and cathode, and the conversion of $NH_4^+$ to $NH_3$ in the vicinity of the cathode, which

could drive a concentration gradient between the two chambers. However, since the pH of the catholyte never exceeded the pKa value for $NH_4^+$ (only along the cathode surface), back diffusion of $NH_4^+$ across the CEM is possible, which would reduce the concentration of $NH_4^+$ in the catholyte. Ultimately, the concentration of $NH_4^+$ in the catholyte is a function of the balance between the electrical potential energy imposed by the electrochemical system, and chemical potential energy imposed by the concentration gradient across the CEM.[72]

**Conversion of ammonium to ammonia** In addition to providing a driving force for ion transfer, the current also helps in splitting water to effectively modify the pH in both chambers. On the ECM cathode, the following reaction takes place[73]:

$$H_2O + e^- \rightarrow \frac{1}{2}H_2 + OH^- \quad (8)$$

Assuming the applied current only triggers water electrolysis, pH along the surface can be calculated as a function of the applied current density (j), and the diffusion of $H^+$ and $OH^-$ within the diffusion boundary layer (where ion convection can be neglected) as given by (eq. 9)[74,75]:

$$j = \frac{F}{\delta}\left[D_{H^+}(c^s_{H^+} - c^b_{H^+}) - D_{OH^-}K_w\left(\frac{1}{c^s_{H^+}} - \frac{1}{c^b_{H^+}}\right)\right] \quad (9)$$

Where, F is the Faraday's constant, δ is the boundary layer thickness, $D_i$ is the diffusion coefficient and $c_i$ the concentration of species i and $K_w$ the ionic product of water. Eq. 9 can be used to calculate the pH along the cathode surface at the applied current density. For current densities of ~17A/m², the pH along the cathode at a distance of *30 μm* from the surface was calculated to be approximately ~13.8, considerably higher than the pKa of ammonium (eq. 1) required to shift the equilibrium toward producing ammonia.

Figures 3c and 3d show the pH trend in the anolyte and catholyte. The pH in the anode chamber varies between 7.38 ± 0.04 – 7.6 ±0.2 over 6 h for all three membranes. It is likely that the carbonate ions in the anolyte act as a buffer to help maintain the anode pH.[69,76] The pH of the catholyte increased from 5.9 ± 0.47 to 7.75 ± 0.35 for CNT ECM, while for 6h Ni and 24h Ni ECMs the pH increases from 6.42 ± 0.3 to 8.5 ± 0.05. For all three ECMs, pH of the catholyte was lower than that calculated. The theoretical pH was calculated for a very thin slice of water along the membrane surface (30 μm), due to proton migration from the anolyte and the large volume of the catholyte, the bulk pH in the catholyte showed only a mild increase.

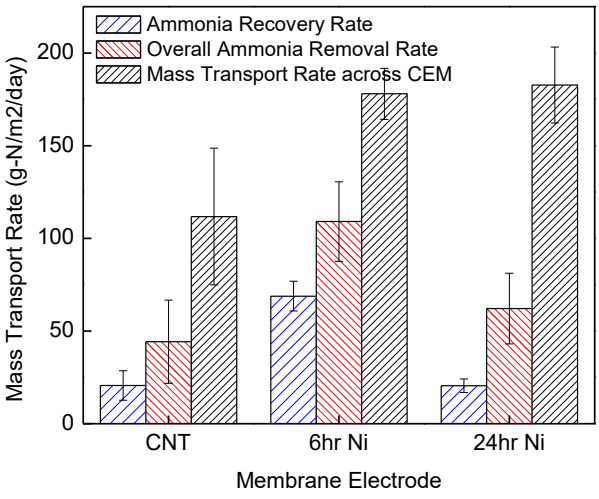


**Figure 4.** Comparing nitrogen flux across the CEM with overall ammonia removal and recovery rate for each ECM.

**Transport and recovery of ammonia** In this study, ammonium transport across the ECM represents $NH_3$-N recovery. Figure 4 shows the ammonia transport rate for all three membranes. The mass transport across the CEM is lower than previously reported, likely due to the low electrical current to ammonia loading ratio. In our work, we applied a current density of ~17 A/m² and an ammonia loading of 0.7 gN/L. In comparison, Tarpeh et al. used a three electrode set-up with metal electrodes to achieve a current density of 100A/m², and the $NH_4^+$ transfer across the CEM was calculated to be 1710

gN/m$^2$/d, while Christiaens et al. used a (bio)electrochemical cell to achieve a $NH_4^+$ transfer of 63.632 gN/m$^2$ with a current density of 48 A/m2.[47,49] Although transport across the CEM is current limited, the mass transport of $NH_3$-N across the CEM is higher than that across the ECM, leading to the accumulation of ammonium in the catholyte. Of course, the accumulation of ammonium in the catholyte is strongly dependent on the membrane area (both the CEM and ECM), with larger ECM areas enabling larger mass removal.

Figure 4 also compares the overall $NH_3$-N removal rate (i.e., $NH_3$-N removed from the anolyte) with the $NH_3$-N recovery rate (i.e., $NH_3$-N that passed through the ECM and accumulated in the acid solutions). CNT and 6h Ni ECMs show the highest percentage of $NH_3$-N recovery (% of ammonia recovered in acid solution over total ammonia removed from the catholyte), ~65 %, while the percent of $NH_3$-N recovered is ~21% for 24h Ni ECM. However, the $NH_3$-N recovery rate was the highest for the 6h Ni ECM (68.86 ±8.02 g-N/m2/day), while it was similar for 24h Ni and CNT ECM (20.51 ±3.69 g-N/m$^2$/d and 26.06 ±0.87 g-N/m$^2$/d, respectively). Lower recovery by 24h Ni ECM could be attributed to its lower gas permeability, a result of the longer nickel deposition time that increased pore blocking. The recovery rate measured in our experiments was higher than that of reported in other studies utilizing an electrical current to facilitate the conversion of ammonium to ammonia gas. For example, Hou et. al. reported a recovery rate of 36.2 g-N/m$^2$/d for a Nickel membrane electrode, while Zhang et. al. recovered ammonia using a carbon slurry in a capacitive desalination unit, with a reported recovery rate of 19.5 g-N/m$^2$/d at a current density of 17.2 A/m$^2$.[18,48]

A mass balance on $NH_3$-N shows a significant amount of unaccounted ammonia. As discussed above, of the total amount of ammonia removed, between 35–79% is unaccounted for. We speculate that the unaccounted ammonia volatilized and is either present in the headspace or escaped from the acid stripping solution. The ammonia loss was also measured by checking for nitrate/nitrite formation. Measurement revealed no nitrate or nitrite formation in either solution (anolyte or cathoyte). Moreover, total nitrogen concentration matched the concentration of $NH_3$-N leading us to conclude that ammonia in the catholyte was either recovered as ammonium sulfate (i.e, passed through the ECM), volatilized, or remained in solution.[48]

**Vacuum extraction of ammonia**

For recovering ammonia with vacuum as the driving force, 6h Ni ECM was used for its improved performance compared to the other membranes. Figure 5 shows an $NH_3$-N removal rate of ~62 ±15.30 g-N/m$^2$/d, and a recovery of ~17.56 ±5.60 g-N/m$^2$/d. Similar to the acid circulation experiments, the mass transport of $NH_3$-N across the CEM was much higher than the mass transport across the ECM, demonstrating the importance of the ECM area.

Gas transfer across a highly porous membrane occurs mainly by Knudsen diffusion, and as a result, the permeability of the transporting species depends on the geometry and structure of the membrane, and on the molecular weight of the permeating species.[35,77] Most notably, the mass flux across the membrane is directly proportional to the pressure difference across the membrane.[78]

Flux of ammonia, J, through the ECM under an applied vacuum can be described by (Equation 10) [26,78,79]:

$$J = \alpha * (P_{fNH_3} - P_v Y_{vNH_3}) \quad \text{[mol/m}^2\text{/s]} \qquad (10)$$

Where, α is the membrane permeability coefficient, $P_{fNH_3}$ is the partial pressure of ammonia on the feed side, $P_v$, the vacuum pressure on the permeate side, and $Y_{vNH3}$ the mole fraction in vapor phase on the vacuum side. The partial pressure of ammonia at the feed side, $P_{fNH_3}$, can be calculated using Henry's law as (Equation 11)[26]:

$$P_{fNH_3} = \frac{100*\gamma*m_{NH_3}}{K_H} \text{ [kPa]} \quad (11)$$

Where, $m_{NH_3}$ is the molality of ammonia in the feed, γ is the activity coefficient, and $K_H$ the Henry's constant for ammonia. Assuming an activity coefficient of 1 and a Henry's constant of 55.96 mol/(Kg atm) at 25ºC, the partial pressure of ammonia on the feed side is calculated to be 0.0271 in Hg. Therefore, mass transfer of ammonia under vacuum is inhibited by its high Henry's constant, which is responsible for the low partial pressure.[14,40,49,72] This effect is enhanced due to the external applied potential that causes other cations in solution to compete with $NH_4^+$ ion migration to the cathode (ECM) surface.[80]Ammonia transfer is also affected by flux of water vapor and hydrogen gas across the ECM.[18,26,41,81]

The overall $NH_3$-N removal rate for the vacuum experiments is considerably lower than that measured using the circulating acid solution. The disparity in the recovery and removal rates for vacuum and acid circulation can be attributed to the higher driving force for systems using acid solutions, which provide an essentially infinite sink for ammonia transfer. Figure 5 shows that at the applied vacuum, 30% of the $NH_3$-N is recovered compared to the 63% recovery for experiments with circulating acid solution. $NH_3$-N recovery could therefore be improved by applying a higher vacuum, provided the ECM does not wet under the applied pressure.

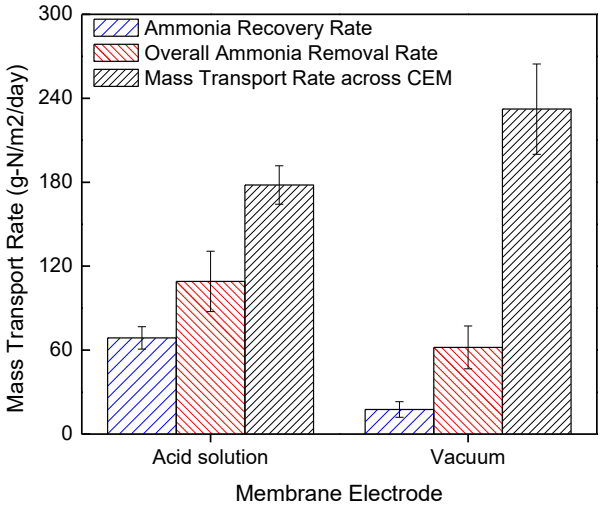


**Figure 5.** Comparing mass transport rates for 6h-Ni membrane for the two experimental setups to extract ammonia, circulating acid solution and vacuum.

**Energy Consumption**

The energy consumption for the ECMs was ~40% lower than conventional nitrogen removal processes such as the nitrification-denitrification process (12.5 kWh/Kg-N).[82] Although this energy consumption is higher than that associated with the Annamox process (4.4-5.3 kWh/Kg-N), the current process benefits as it recovers nitrogen as ammonia, a valuable commodity.[71,82] The specific energy demand based on ammonia recovered in the stripping solution was 7.0±2.40 kWh/kg $NH_3$-N for the CNT coated membrane, and 7.06±1.06 kWh/kg $NH_3$-N for the 6h Ni membrane. However, for the 24h Ni membrane, due to its low ammonium recovery, the specific energy demand was significantly higher (20.45±6.25 kWh/kg$NH_3$-N). Energy consumption of the process can be further lowered if the unaccounted ammonia, likely present in the headspace, is also recovered. Based on total ammonia removal (ammonia recovered using stripping solution and the missing ammonia that is likely volatilized), the energy consumption of the process is reduced by 35–74%, to 3.66±0.94 kWh/kg $NH_3$-N for the CNT coated membrane, 4.53±0.77

kWh/kg $NH_3$-N for the 6h Ni membrane, and 5.28±2.64 kWh/kg $NH_3$-N for the 24h Ni membrane.

For $NH_3$-N recovery via vacuum, the specific energy requirement based on $NH_3$-N removed was 11.68±2.8 kWh/Kg-N, which is 22.3% lower than the amount of energy required to produce ammonia via the Haber-Bosch process in a large scale commercial installation. However, the amount of ammonia actually recovered in the vacuum trap was much lower than the amount of ammonia removed, driving up the specific energy costs. The decrease is ammonia recovery could be attributed to insufficient vacuum due to the very low vapor pressure of ammonia, high Henry constant, and incompatibility of the vacuum pump with ammonia leading to decline in pump performance over time. Thus, work is still needed to develop better vacuum extraction methods capable of overcoming ammonia's high solubility (and low partial vapor pressure) to recover ammonia with reduced specific energy requirements.

## Conclusions

In this study, three electrically conductive membrane materials: (i) CNT coated ECM, (ii) 6h-Ni ECM, and (ii) 24h-Ni ECM were studied for their ammonia recovery capacities. The 6h-Ni ECM showed superior performance with high current densities and minimal pore blocking. Ammonia recovery via electrochemical methods is highly dependent on the current in the system. The applied current density influences the mass transport of ammonia across the cation exchange membrane as well as the pH along the cathode surface. Furthermore, using a gas permeable membrane to recover ammonia is a mass transport limited process, amplified further when using vacuum to provide the driving force for ammonia recovery (due to high Henry constant for ammonia).

The energy consumption of the ammonia recovery process, for our system, was lower than some conventional nitrogen removal processes, however, recovering all ammonia being removed from the system (ammonia volatilized/present in headspace), would greatly benefit the specific energy requirement.

## Conflicts of interest

There are no conflicts to declare.

## Acknowledgements

We would like to thank BARD US-Israel Agricultural Research and Development Fund (US-5051-17), and the US Department of Agriculture (2017-67022-26135).

## Notes and references

(1) Rasul, G.; Sharma, B. The Nexus Approach to Water–Energy–Food Security: An Option for Adaptation to Climate Change. *Clim. Policy* **2016**, *16* (6), 682–702.

(2) Bazilian, M.; Rogner, H.; Howells, M.; Hermann, S.; Arent, D.; Gielen, D.; Steduto, P.; Mueller, A.; Komor, P.; Tol, R. S. J.; Yumkella, K. K. Considering the Energy, Water and Food Nexus: Towards an Integrated Modelling Approach. *Energy Policy* **2011**, *39* (12), 7896–7906.

(3) Allan, T.; Keulertz, M.; Woertz, E. The Water–Food–Energy Nexus: An Introduction to Nexus Concepts and Some Conceptual and Operational Problems. *Int. J. Water Resour. Dev.* **2015**, *31* (3), 301–311.

(4) Xie, M.; Shon, H. K.; Gray, S. R.; Elimelech, M. Membrane-Based Processes for Wastewater Nutrient Recovery: Technology, Challenges, and Future Direction. *Water Res.* **2016**, *89*, 210–221.

(5) Rulkens, W. H.; Klapwijk, A.; Willers, H. C. Recovery of Valuable Nitrogen Compounds from Agricultural Liquid Wastes: Potential Possibilities, Bottlenecks and Future Technological Challenges. *Environ. Pollut.* **1998**, *102* (SUPPL. 1), 727–735.

(6) Cai, T.; Park, S. Y.; Li, Y. Nutrient Recovery from Wastewater Streams by Microalgae: Status and Prospects. *Renew. Sustain. Energy Rev.* **2013**, *19*, 360–369.

(7) Afif, A.; Radenahmad, N.; Cheok, Q.; Shams, S.; Kim, J. H.; Azad, A. K. Ammonia-Fed Fuel Cells: A Comprehensive Review. *Renew. Sustain. Energy Rev.* **2016**, *60*, 822–835.

(8) Zamfirescu, C.; Dincer, I. Ammonia as a Green Fuel and Hydrogen Source for Vehicular Applications. *Fuel Process. Technol.* **2009**, *90* (5), 729–737.

(9) Yan, T.; Ye, Y.; Ma, H.; Zhang, Y.; Guo, W.; Du, B.; Wei, Q.; Wei, D.; Ngo, H. H. A Critical Review on Membrane Hybrid System for Nutrient Recovery from Wastewater. *Chem. Eng. J.* **2018**, *348* (April), 143–156.

(10) Batstone, D. J.; Hülsen, T.; Mehta, C. M.; Keller, J. Platforms for Energy and Nutrient Recovery from Domestic Wastewater: A Review. *Chemosphere* **2015**, *140*, 2–11.

(11) Cheng, J. J.; Stomp, A. M. Growing Duckweed to Recover Nutrients from Wastewaters and for Production of Fuel Ethanol and Animal Feed. *Clean - Soil, Air, Water* **2009**, *37* (1), 17–26.

(12) Wang, Y.; Huang, X.; Yuan, Q. Nitrogen and Carbon Removals from Food Processing Wastewater by an Anoxic/Aerobic Membrane Bioreactor. *Process Biochem.* **2005**, *40* (5), 1733–1739.

(13) Cordell, D.; Drangert, J. O.; White, S. The Story of Phosphorus: Global Food Security and Food for Thought. *Glob. Environ. Chang.* **2009**, *19* (2), 292–305.

(14) Muster, T. H.; Jermakka, J. Electrochemically-Assisted Ammonia Recovery from Wastewater Using a Floating Electrode. *Water Sci. Technol.* **2017**, *75* (8), 1804–1811.

(15) Zhang, C.; Ma, J.; He, D.; Waite, T. D. Capacitive Membrane Stripping for Ammonia Recovery (CapAmm) from Dilute Wastewaters. *Environ. Sci. Technol. Lett.* **2017**, acs.estlett.7b00534.

(16) Pfromm, P. H. Towards Sustainable Agriculture: Fossil-Free Ammonia. *J. Renew. Sustain. Energy* **2017**, *9* (3).

(17) Rosso, D.; Larson, L. E.; Stenstrom, M. K. Aeration of Large-Scale Municipal Wastewater Treatment Plants: State of the Art. *Water Sci. Technol.* **2008**, *57* (7), 973–978.

(18) Hou, D.; Iddya, A.; Chen, X.; Wang, M.; Ding, Y.; Jassby, D.; Ren, Z. J. *Nickel Based Membrane Electrodes Enable High Rate Electrochemical Ammonia Recovery*; 2018.

(19) Dewil, R.; Baeyens, J.; Goutvrind, R. Ultrasonic Treatment of Waste Activated Sludge. *Environ. Prog.* **2006**, *25* (2), 121–128.

(20) Liu, Y. Chemically Reduced Excess Sludge Production in the Activated Sludge Process. *Chemosphere* **2003**, *50* (1), 1–7.

(21) Shin, C.; McCarty, P. L.; Kim, J.; Bae, J. Pilot-Scale Temperate-Climate Treatment of Domestic Wastewater with a Staged Anaerobic Fluidized Membrane Bioreactor (SAF-MBR). *Bioresour. Technol.* **2014**, *159*, 95–103.

(22) Harb, M.; Hong, P. Anaerobic Membrane Bioreactor Effluent Reuse: A Review of Microbial Safety Concerns. *Fermentation* **2017**, *3* (3), 39.

(23) Lettinga, G.; Field, J.; Van Lier, J.; Zeeman, G.; Hulshoff Pol, L. W. Advanced Anaerobic Wastewater Treatment in the near Future. *Water Sci. Technol.* **1997**, *35* (10), 5–12.

(24) Kartal, B.; Kuenen, J. G.; Van Loosdrecht, M. C. M. Sewage Treatment with Anammox. *Science (80-. ).* **2010**, *328* (5979), 702–703.

(25) Strous, M.; Van Gerven, E.; Zheng, P.; Kuenen, J. G.; Jetten, M. S. M. Ammonium Removal from Concentrated Waste Streams with the Anaerobic Ammonium Oxidation (Anammox) Process in Different Reactor Configurations. *Water Res.* **1997**, *31* (8), 1955–1962.

(26) He, Qingyao, Tu, Te, Yan, Shuiping, Yang, Xing, Duke, Mikel, Zhang, Yanlin, Zhao, S. Relating Water Vapor Transfer to Ammonia Recovery from Biogas Slurry by Vacuum Membrane Distillation. *Sep. Purif. Technol.* **2018**, *191*, 182–191.

(27) Masse, L.; Massé, D. I.; Pellerin, Y.; Dubreuil, J. Osmotic Pressure and Substrate Resistance during the Concentration of Manure Nutrients by Reverse Osmosis Membranes. *J. Memb. Sci.* **2010**, *348* (1–2), 28–33.

(28) Bonmatı, A.; Flotats, X. Air Stripping of Ammonia from Pig Slurry: Characterisation and Feasibility as a Pre- or Post-Treatment to Mesophilic Anaerobic Digestion. *Waste Manag.* **2003**, *23*, 261–272.

(29) Wendong Tao ⇑, A. T. U. Coupling Thermal Stripping and Acid Absorption for Ammonia Recovery from Dairy Manure: Ammonia Volatilization Kinetics and Effects of Temperature, PH and Dissolved Solids Content. *Chem. Eng. J.* **2015**, *280*, 188–196.

(30) Milan, Z.; Sánchez, E.; Weiland, P.; De Las Pozas, C.; Borja, R.; Mayari, R.; Rovirosa, N. Ammonia Removal from Anaerobically Treated Piggery Manure by Ion Exchange in Columns Packed with Homoionic Zeolite. *Chem. Eng. J.* **1997**, *66* (1), 65–71.

(31) Uludag-Demirer, S.; Demirer, G. N.; Chen, S. Ammonia Removal from Anaerobically Digested Dairy Manure by Struvite Precipitation. *Process Biochem.* **2005**, *40* (12), 3667–3674.

(32) Etter, B.; Tilley, E.; Khadka, R.; Udert, K. M. Low-Cost Struvite Production Using Source-Separated Urine in Nepal. *Water Res.* **2011**, *45* (2), 852–862.

(33) Jordaan, E. M.; Ackerman, J.; Cicek, N. Phosphorus Removal from Anaerobically Digested Swine Wastewater through Struvite Precipitation. *Water Sci. Technol.* **2010**, *61* (12), 3228–3234.

(34) Hou, D.; Jassby, D.; Nerenberg, R.; Ren, Z. J. Hydrophobic Gas Transfer Membranes for Wastewater Treatment and Resource Recovery. *Environ. Sci. Technol.* **2019**, *53*, 11618–11635.

(35) EL-Bourawi, M. S.; Khayet, M.; Ma, R.; Ding, Z.; Li, Z.; Zhang, X. Application of Vacuum Membrane Distillation for Ammonia Removal. *J. Memb. Sci.* **2007**, *301* (1–2), 200–209.

(36) Malaisamy, R.; Talla-Nwafo, A.; Jones, K. L. Polyelectrolyte Modification of Nanofiltration Membrane for Selective Removal of Monovalent Anions. *Sep. Purif. Technol.* **2011**, *77* (3), 367–374.

(37) Tran, A. T. K.; Zhang, Y.; Lin, J.; Mondal, P.; Ye, W.; Meesschaert, B.; Pinoy, L.; Van Der Bruggen, B. Phosphate Pre-Concentration from Municipal Wastewater by Selectrodialysis: Effect of Competing Components. *Sep. Purif. Technol.* **2015**, *141*, 38–47.

(38) Mckinney, R.; Rhodes, J. H. Aromatic Polyamide Membranes for Reverse Osmosis Separations. *Macromolecules* **1971**, *4* (5), 633–637.

(39) Candido, L.; Gomes, J. A. C. P. Evaluation of Anode Materials for the Electro-Oxidation of Ammonia and Ammonium Ions. *Mater. Chem. Phys.* **2011**, *129* (3), 1146–1151.

(40) Renard, J. J.; Calidonna, S. E.; Henley, M. V. Fate of Ammonia in the Atmosphere - A Review for Applicability to Hazardous Releases. *J. Hazard. Mater.* **2004**, *108* (1–2), 29–60.

(41) Ding, Z.; Liu, L.; Li, Z.; Ma, R.; Yang, Z. Experimental Study of Ammonia Removal from Water by Membrane Distillation ( MD ): The Comparison of Three Configurations. *J. Memb. Sci.* **2006**, *286*, 93–103.

(42) M. J. Rothrock Jr.; A. A. Szögi; M. B. Vanotti. Recovery of Ammonia from Poultry Litter Using Gas-Permeable Membranes. *Trans. ASABE* **2010**, *53* (4), 1267–1275.

(43) Kuntke, P.; Zamora, P.; Saakes, M.; Buisman, C. J. N.; Hamelers, H. V. M. Gas-Permeable Hydrophobic Tubular Membranes for Ammonia Recovery in Bio-Electrochemical Systems. *Environ. Sci. Water Res. Technol.* **2016**, *2* (2), 261–265.

(44) Emerson, K.; Russo, R.; Lund, R.; Thurston, R. Aqueous Ammonia Equilibrium Calculations: Effect of PH and Temperature. *J. Fish. Res. Board Canada* **1975**, *32* (12), 2379–2383.

(45) Rothrock, M. J.; Szögi, A. A.; Vanotti, M. B. Recovery of Ammonia from Poultry Litter Using Flat Gas Permeable Membranes. *Waste Manag.* **2013**, *33* (6), 1531–1538.

(46) Kartohardjono, S.; Fermi, M. I.; Yuliusman; Elkardiana, K.; Sangaji, A. P.; Ramadhan, A. M. The Removal of Dissolved Ammonia from Wastewater through a Polypropylene Hollow Fiber Membrane Contactor. *Int. J. Technol.* **2015**, *6* (7), 1146–1152.

(47) Christiaens, M. E. R.; Gildemyn, S.; Matassa, S.; Ysebaert, T.; De Vrieze, J.; Rabaey, K. Electrochemical Ammonia Recovery from Source-Separated Urine for Microbial Protein Production. *Environ. Sci. Technol.* **2017**, *51* (22), 13143–13150.

(48) Zhang, C.; Ma, J.; He, D.; Waite, T. D. Capacitive Membrane Stripping for Ammonia Recovery (CapAmm) from Dilute Wastewaters. *Environ. Sci. Technol. Lett.* **2017**, acs.estlett.7b00534.

(49) Tarpeh, W. A.; Barazesh, J. M.; Cath, T. Y.; Nelson, K. L. Electrochemical Stripping to Recover Nitrogen from Source-Separated Urine. *Environ. Sci. Technol.* **2018**, *52* (3), 1453–1460.

(50) Luther, A. K.; Desloover, J.; Fennell, D. E.; Rabaey, K. Electrochemically Driven Extraction and Recovery of Ammonia from Human Urine. *Water Res.* **2015**, *87*, 367–377.

(51) TERADA, A.; HIBIYA, K.; NAGAI, J.; TSUNEDA, S.; HIRATA, A. Nitrogen Removal Characteristics and Biofilm Analysis of a Membrane-Aerated Biofilm Reactor Applicable to High-Strength Nitrogenous Wastewater Treatment. *J. Biosci. Bioeng.* **2003**, *95* (2), 170–178.

(52) Lu, L.; Huang, Z.; Rau, G. H.; Ren, Z. J. Microbial Electrolytic Carbon Capture for Carbon Negative and Energy Positive Wastewater Treatment. *Environ. Sci. Technol.* **2015**, *49* (13), 8193–8201.

(53) Tang, L.; Iddya, A.; Zhu, X.; Dudchenko, A. V.; Duan, W.; Turchi, C.; Vanneste, J.; Cath, T. Y.; Jassby, D. Enhanced Flux and Electrochemical Cleaning of Silicate Scaling on Carbon Nanotube-Coated Membrane Distillation Membranes Treating Geothermal Brines. *ACS Appl. Mater. Interfaces* **2017**, *9* (44).

(54) Ukwuani, A. T.; Tao, W. Developing a Vacuum Thermal Stripping – Acid Absorption Process for Ammonia Recovery from Anaerobic Digester Effluent. *Water Res.* **2016**, *106*, 108–115.

(55) Khayet, M. Membranes and Theoretical Modeling of Membrane Distillation: A Review. *Adv. Colloid Interface Sci.* **2011**, *164* (1–2), 56–88.

(56) Tomaszewska, M. Preparation and Properties of Flat-Sheet Membranes from Poly(Vinylidene Fluoride) for Membrane Distillation. *Desalination* **1996**, *104* (1–2), 1–11.

(57) Zhou, Y.; Sun, C.; Yang, X.; Zou, G.; Wu, H.; Xi, S. Flame-like Ni(OH) 2 Strongly Promotes the Dissociation of Water and Can Be Used to Produce an Excellent Hybrid Electrocatalyst for the Hydrogen Evolution Reaction in Alkaline Media. *Electrochem. commun.* **2018**, *91* (May), 66–70.

(58) Gong, M.; Zhou, W.; Tsai, M. C.; Zhou, J.; Guan, M.; Lin, M. C.; Zhang, B.; Hu, Y.; Wang, D. Y.; Yang, J.; Pennycook, S. J.; Hwang, B. J.; Dai, H. Nanoscale Nickel Oxide/Nickel Heterostructures for Active Hydrogen Evolution Electrocatalysis. *Nat. Commun.* **2014**, *5*, 1–6.

(59) Grdeń, M.; Alsabet, M.; Jerkiewicz, G. Surface Science and Electrochemical Analysis of Nickel Foams. *ACS Appl. Mater. Interfaces* **2012**, *4* (6), 3012–3021.

(60) Yu, X.; Hua, T.; Liu, X.; Yan, Z.; Xu, P.; Du, P. Nickel-Based Thin Film on Multiwalled Carbon Nanotubes as an Efficient Bifunctional Electrocatalyst for Water Splitting. *ACS Appl. Mater. Interfaces* **2014**, *6* (17), 15395–15402.

(61) Hou, D.; Feng, L.; Zhang, J.; Dong, S.; Zhou, D.; Lim, T. T. Preparation, Characterization and Performance of a Novel Visible Light Responsive Spherical Activated Carbon-Supported and Er 3+ :YFeO 3 -Doped TiO 2 Photocatalyst. *J. Hazard. Mater.* **2012**, *199–200*, 301–308.

(62) Xu, C.; Zhou, J. bo; Zeng, M.; Fu, X. ling; Liu, X. jiang; Li, J. ming. Electrodeposition Mechanism and Characterization of Ni–Mo Alloy and Its Electrocatalytic Performance for Hydrogen Evolution. *Int. J. Hydrogen Energy* **2016**, *41* (31), 13341–13349.

(63) Fan, C.; Piron, D. L.; Paradis, P. Hydrogen Evolution on Electrodeposited Nickel-Cobalt-Molybdenum in Alkaline Water Electrolysis. *Electrochim. Acta* **1994**, *39* (18), 2715–2722.

(64) Mitov, M.; Chorbadzhiyska, E.; Nalbandian, L.; Hubenova, Y. Nickel-Based Electrodeposits as Potential Cathode Catalysts for Hydrogen Production by Microbial Electrolysis. *J. Power Sources* **2017**, *356*, 467–472.

(65) Shetty, S.; Mohamed Jaffer Sadiq, M.; Bhat, D. K.; Hegde, A. C. Electrodeposition and Characterization of Ni-Mo Alloy as an Electrocatalyst for Alkaline Water Electrolysis. *J. Electroanal. Chem.* **2017**, *796* (May), 57–

65.
(66) Tilley, S. D.; Mayer, M. T.; Park, N.-G.; Luo, J.; Gratzel, M.; Fan, H. J.; Schreier, M.; Nazeeruddin, M. K.; Im, J.-H. Water Photolysis at 12.3% Efficiency via Perovskite Photovoltaics and Earth-Abundant Catalysts. *Science (80-. ).* **2014**, *345* (6204), 1593–1596.
(67) Li, Z.-F.; Wang, Y.; Botte, G. G. Revisiting the Electrochemical Oxidation of Ammonia on Carbon-Supported Metal Nanoparticle Catalysts. *Electrochim. Acta* **2017**, *228*, 351–360.
(68) Binninger, T.; Fabbri, E.; Kötz, R.; Schmidt, T. J. Determination of the Electrochemically Active Surface Area of Metal-Oxide Supported Platinum Catalyst. *J. Electrochem. Soc.* **2013**, *161* (3), H121–H128.
(69) Cord-Ruwisch, R.; Law, Y.; Cheng, K. Y. Ammonium as a Sustainable Proton Shuttle in Bioelectrochemical Systems. *Bioresour. Technol.* **2011**, *102* (20), 9691–9696.
(70) Rodríguez Arredondo, M.; Kuntke, P.; ter Heijne, A.; Hamelers, H. V. M.; Buisman, C. J. N. Load Ratio Determines the Ammonia Recovery and Energy Input of an Electrochemical System. *Water Res.* **2017**, *111*, 330–337.
(71) Kuntke, P.; Sleutels, T. H. J. A.; Arredondo, M. R.; Georg, S.; Barbosa, S. G.; Heijne, A. ( Bio ) Electrochemical Ammonia Recovery : Progress and Perspectives. *Appl. Microbiol. Biotechnol.* **2018**, *2*, 3865–3878.
(72) Dykstra, J. E.; Biesheuvel, P. M.; Bruning, H.; Ter Heijne, A. Theory of Ion Transport with Fast Acid-Base Equilibrations in Bioelectrochemical Systems. *Phys. Rev. E - Stat. Nonlinear, Soft Matter Phys.* **2014**, *90* (1), 1–10.
(73) Popat, S. C.; Ki, D.; Rittmann, B. E.; Torres, C. I. Importance of OH-Transport from Cathodes in Microbial Fuel Cells. *ChemSusChem* **2012**, *5* (6), 1071–1079.
(74) Biedermann, P. U.; Auinger, M.; Mayrhofer, K. J. J.; Katsounaros, I.; Klemm, S. O.; Topalov, A. A.; Meier, J. C.; Rohwerder, M. Near-Surface Ion Distribution and Buffer Effects during Electrochemical Reactions. *Phys. Chem. Chem. Phys.* **2011**, *13* (36), 16384.
(75) Katsounaros, I.; Meier, J. C.; Klemm, S. O.; Topalov, A. A.; Biedermann, P. U.; Auinger, M.; Mayrhofer, K. J. J. The Effective Surface PH during Reactions at the Solid-Liquid Interface. *Electrochem. commun.* **2011**, *13* (6), 634–637.
(76) Cohen, Y. *Nutrient Recovery from Wastewater*; Svedish University of Agricultural Sciences, 2015.
(77) Abu-Zeid, M. A. E. R.; Zhang, Y.; Dong, H.; Zhang, L.; Chen, H. L.; Hou, L. A Comprehensive Review of Vacuum Membrane Distillation Technique. *Desalination* **2015**, *356*, 1–14.
(78) Izquierdo-Gil, M. A.; Jonsson, G. Factors Affecting Flux and Ethanol Separation Performance in Vacuum Membrane Distillation (VMD). *J. Memb. Sci.* **2003**, *214* (1), 113–130.
(79) Abu-Zeid, M. A. E. R.; Zhang, Y.; Dong, H.; Zhang, L.; Chen, H. L.; Hou, L. A Comprehensive Review of Vacuum Membrane Distillation Technique. *Desalination*. Elsevier B.V. 2015, pp 1–14.
(80) Chiam, C. K.; Sarbatly, R. Vacuum Membrane Distillation Processes for Aqueous Solution Treatment-A Review. *Chem. Eng. Process. Process Intensif.* **2014**, *74*, 27–54.
(81) Lu, L.; Hou, D.; Wang, X.; Jassby, D.; Ren, Z. J. Active H 2 Harvesting Prevents Methanogenesis in Microbial Electrolysis Cells. *Environ. Sci. Technol. Lett.* **2016**, *3* (8), 286–290.
(82) Kuntke, P.; Sleutels, T. H. J. A.; Saakes, M.; Buisman, C. J. N. Hydrogen Production and Ammonium Recovery from Urine by a Microbial Electrolysis Cell. *Int. J. Hydrogen Energy* **2014**, *39* (10), 4771–4778.

 

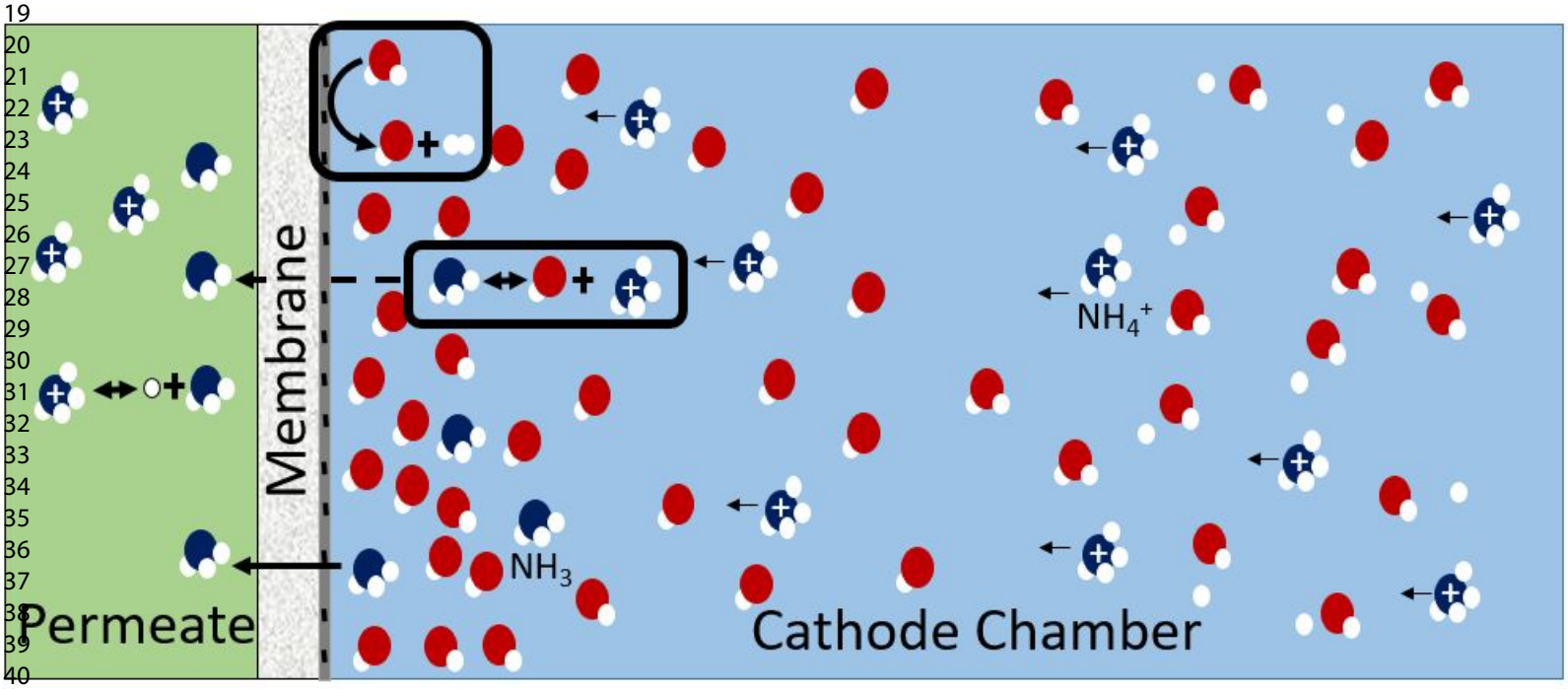
Membrane
$NH_4^+$
$NH_3$
Permeate
Cathode Chamber